[논 문] 한국재료학회지
Korean J. Mater. Res.
Vol. 25, No. 11 (2015)
http://dx.doi.org/10.3740/MRSK.2015.25.11.612

On-Site Corrosion Behavior of T91 Steel after Long-Term Service in Power Plant

Yinsheng He, Jungchel Chang[1], Je-Hyun Lee and Keesam Shin[†]

School of Nano & Advanced Materials Engineering, Changwon National University, Changwon 51140, Korea
[1]Technology Policy and Planning Department, Korea Electric Power Corporation, Naju 58217, Korea

(Received July 27, 2015 : Revised September 8, 2015 : Accepted October 1, 2015)

Abstract In this work, on-site corrosion behavior of heat resistant tubes of T91, used as components of a superheater in a power plant for up to 25,762 h, has been investigated using scanning electron microscopy(SEM), energy dispersive X-ray spectroscopy (EDS), and electron backscattered diffraction(EBSD), with the objectives of studying the composition, phase distribution, and evolution during service. A multi-layer structure of oxide scale was found on both the steamside and the fireside of the tube surface; the phase distribution was in the order of hematite/magnetite/spinel from the outer to the inner matrix on the steamside, and in the order of slag/magnetite/spinel from the outer to the inner matrix on the fireside. The magnetite layer was found to be rich in pores and cracks. The absence of a hematite layer on the fireside was considered to be due to the low oxygen partial pressure in the corrosion environment. The thicknesses of the hematite and of the slag-deposit layer were found to exhibit no significant change with the increase of the service time.

Key words T91 heat resistant steel, corrosion, oxide scales, SEM, EBSD.

1. Introduction

Grade 91(Gr. 91, ASME T/P91) heat resistant steel, as one of the structural materials, has been broadly employed to superheaters(S/H) and reheaters in fossil-fuel power plants. One of the limiting factors of the application is the corrosion under the ultra-supercritical(USC) water in steamside and rough coal-ash in fireside.[1,2] Oxidation is known as the predominant corrosion phenomena in long-term service of this material. Formation of various oxide layers on the surface not only reduces the thermal exchange efficiency, but also accelerates the creep damage degradation.[3] Various defects(pores, crack) were accompanied with the formation and growth of the oxide scales. During long-term service, these defects grow and spall to form a coarse crack at the interface, resulting in the exfoliation of oxide scales which would flow into the turbine system, causing serious problems to the steam turbines.[4-6] Thus, characterization of the oxide scales in long term service is critical for the control and maintenance of the parts used in power plants. Various researches have been carried out investigations both in laboratory and in field to determine characteristics of the morphology of the oxide layers and the oxidation mechanisms with variations in the time, temperature, alloy composition, dissolved oxygen content, etc.[4,7-11] The objectives of this work are characterization of the oxide scales(morphologies, chemical composition, phase distribution, growth rate) formed during the usage of T91 in the power plants to obtain and accumulate data on the optimum condition for the chemical cleaning of the tubes. The tubes used as the S/H at fossil-fueled power plants up to 25,762 h were extracted and analyzed using SEM/EDS and EBSD.

2. Experimental Procedure

The T91 tubes used as the S/H in fossil power plants in Korea were extracted considering the service time intervals(7,930 h, 16,966 h and 25,762 h). The service steam temperature and pressure were 541 ^{o}C and 40.7 MPa, respectively. The morphology, chemical composition and phase distributions of the oxide scale layer were examined by SEM(JSM-5610, equipped with INCA

[†]Corresponding author
E-Mail : keesam@changwon.ac.kr (K. Shin, Changwon Nat'l Univ.)

EDS). Cross-sectional specimens were mechanically polished and etched with Vilella's reagent(100 ml ethanol + 1 g picric acid + 5 ml HCl). During the SEM observation, EDS line profile and the elements mapping were carried out to determine the elemental distribution of the oxide scale. Besides, backscattered electron(BSE) imaging was also used to analyze the morphology and chemical composition distribution of the layers, since the contrast is highly sensitive to the atomic number of the element. EBSD measurements were carried out on an orientation image microscopy system(TSL OIM facilities) attached on a field emission SEM(FESEM-MIRA II LMH). The cross-sectional specimens for EBSD measurement were prepared by careful finishing of the polishing in colloidal silica for 4 h.

3. Results and Discussion

3.1 *Oxide scale characteristics*

Fig. 1 shows typical BSE images and corresponding EDS line profiles of the new and 25,762 h specimens. In the new specimen, an oxygen rich layer with the thickness up to ~20 μm was observed(Fig. 1a_1 and a_2), which were formed during the fabrication and the subsequent handling of the tubes.[12] Analyses using the BSE imaging revealed that multi-layer oxide scales of different composition were formed on the used specimens. On the steamside, three layers were formed(marked as outer, intermediate and inner in Fig. 1b_1). However, only two layers were obvious in the EDS line profile(Fig. 1b_2), i.e., an Fe/O-rich layer and an /Fe/O/Cr-rich one, indicating that the outer and intermediate layer may have a similar composition, but with different crystallographic orientation, since the contrast of BSE images were also sensitive to the crystal orientation.[13] On the fireside(Fig. 1c_1 and c_2), a more complex structure were observed. A layer of slag-deposit of Ca/S/Al-rich porous outer layer was formed from the coal-ash. Besides, a Fe/O-rich intermediate layer and a Fe/Cr/O-rich transition layer were formed. The morphologies of these oxide layers were also identified from BSE images, i.e., the pores and cracks, of which will be described later.

The EBSD phase maps of the specimens(Fig. 2) clearly show the phase distributions in the oxide layers. Whereas there is a discontinuous magnetite layer on the matrix(α-ferrite) in the new specimen, the outer layer in steamside (Fig. 2b) contains equiaxed hematite grains, which also owned the features of compact and discontinuous(as mark by open arrow). The intermediate magnetite layer has coarse columnar grains with high density of pores and cracks, which are related to the defect type present in the crystal structure which was well explained by Tan et al.[9] The dark region is the unindentified phase by the EBSD analysis. However, it is believed to be chromite phase as the small grains with Cr and O peaks in EDS are typical characteristics of chromite.[1,11] The inner layer is very dense and contained the magnetite and chromite (nano-sized), which was named as the spinel layer[7]

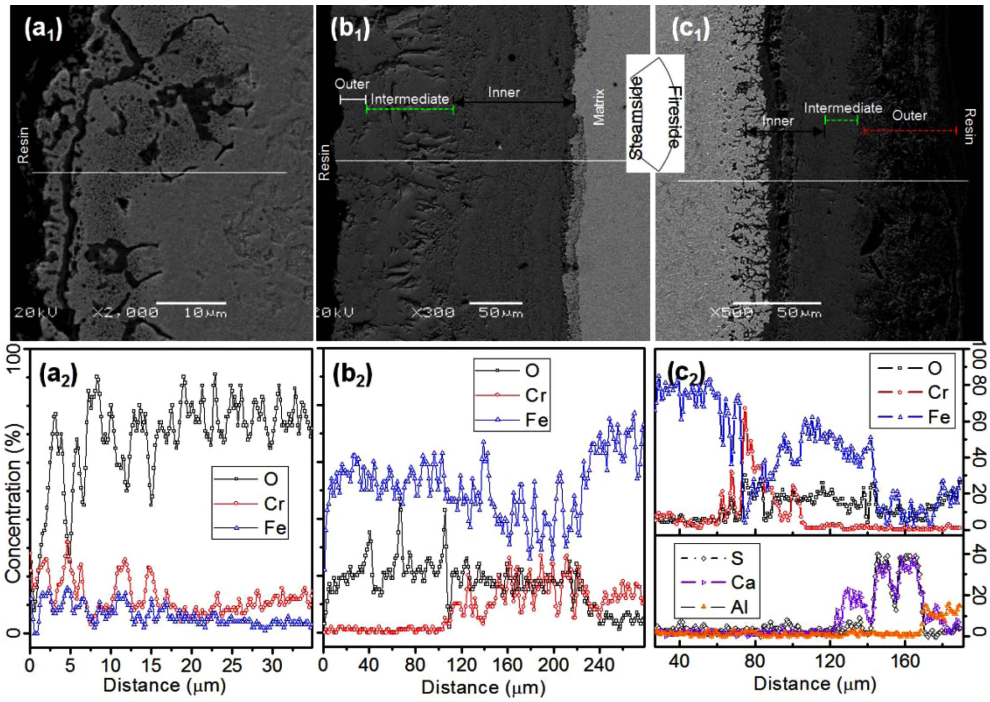

Fig. 1. Typical SEM BSE images (a_1~c_1) and corresponding EDS line profiles (a_2~c_2) of the oxide scale: in the specimens specimens of new (a_1, a_2), and used as S/H for 25,762 h in steamside (b_1, b_2) and fireside (c_1, c_2).

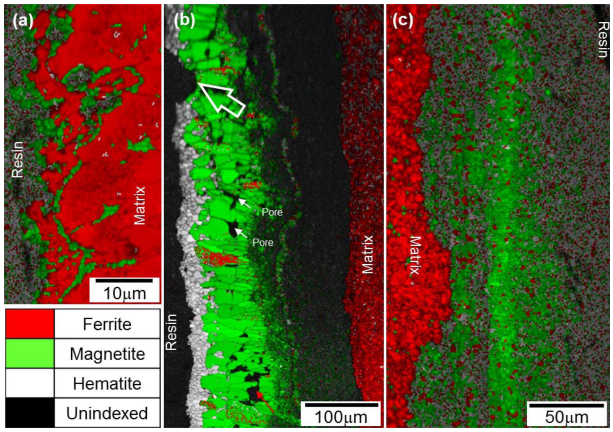

Fig. 2. Typical EBSD phase maps of the oxide scales of the new (a), and the S/H for 25,762 h specimens in steamside (b) and fireside (c).

hereafter(Fig. 2b). In fireside(Fig. 2c), the phase of the outer slag-deposit layer could not be identified by EBSD, due to its honeycomb-like porous structure. Close to slag-deposit layer, a continuous fine and relatively dense magnetite grains layer was formed, which were different from those of the magnetite layer in steamside, suggesting that the formation of magnetite was related to the oxygen partial pressure. A spinel layer was also observed in the inner region next to the matrix. No hematite was formed, which was attributed to the low oxygen partial pressure in the coal-ash atmosphere,[12] since the formation of the hematite was closely related to the oxygen partial pressure.[7]

3.2 *Evolution of scale during service*

Fig. 3 shows the morphologies of the oxide scale in the steamside and fireside of the investigated specimens. The hematite layer and the spinel layer in the steamside were relatively dense, whereas the magnetite layer was with large number of cracks and pores(Fig. $3a_1$~c_1). The cracks and pores were mostly present at the interfaces of magnetite and spinel, and the spinel and internal matrix. Most of the cracks in the magnetite layer were in high angle to the interface, whereas the interface cracks were along with the interface. Similar features to these oxide layers were also observed in the tubes used in the fireside (Fig. $3a_2$~c_2). In the fire side, the slag- deposit layer was not so obvious in the specimen of 7,930 h(Fig. $3b_1$). However, it was very clear in the 16,966 h and in 25,762 h specimens(Fig. $3b_2$ and c_2). Fig. 3 shows that that the phases and their distribution do not change with time, other than the thickness. The characteristics of scale T91 steel is very similar to that of the X20CrMoV12.1, which is also an alloy used widely as a heat resistance alloy.[12]

The thickness of each oxide layer and overall scale were measured and plotted in Fig. 4. Although the thickness of the scale increased with service time, the thickness change of hematite layer in the steamside did not have significant change. In the mean time, the defects in the oxide layer (i.e., pores and cracks) grew also, which will eventually lead to debonding and spalling of the

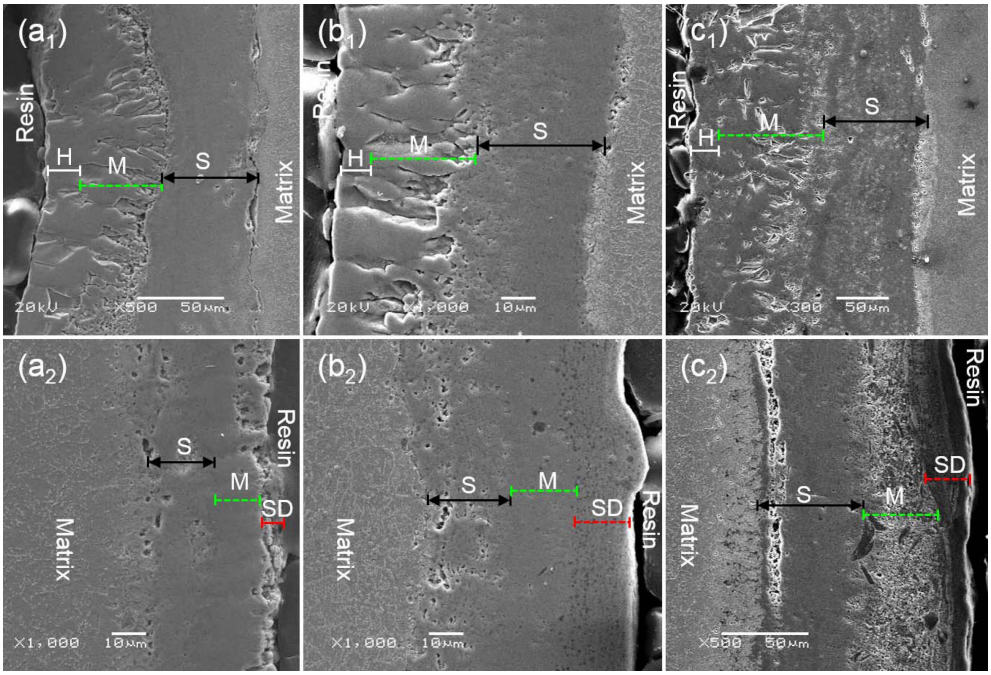

Fig. 3. SEM SE images of the oxide scale on the steamside (a_1~c_1) and fireside (a_2~c_2) of served specimens: (a_1, a_2) 7,930 h, (b_1, b_2) 16,966 h and (c_1, c_2) 25,762 h. *H: hematite, M: magnetite, S: spinel, and SD: slag-deposit.

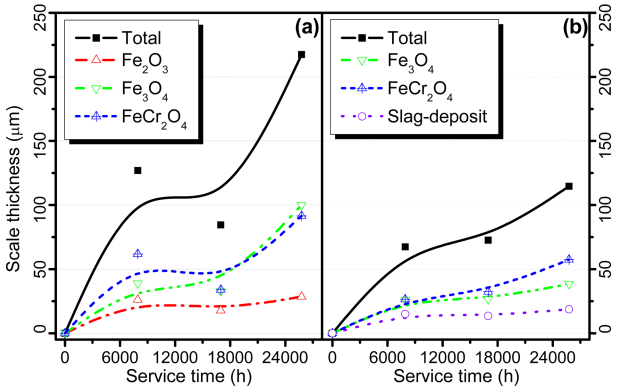

Fig. 4. The effect of the service time on the scale thickness in the steamside (a) and fireside (b).

layers,[11] which was a probable reason of that the thickness of the outer layer(both in steamside and especially in fireside) remains stable upon increase of the service time. As reported by Tan et al.[9] that the growth of the oxide scale of ferritic steel exposed in the USC water was expected to follow the parabolic law $x^2 = k_p t$, where x is the oxide thickness, k_p is the parabolic rate constant, t is the exposure time. However, the on-site growth behavior of the oxide scale is more or less deviated from the parabolic law, and very differed from the results based on the laboratory test results.

4. Conclusion

In this work, the morphology, chemical composition, phase distribution as well as the evolution of the oxide scale formed on the steamside and fireside of the T91 tube after service as S/H up to 25,762 h in power plant were analyzed in detail using SEM/EDS, EBSD. The oxide scales on the steamside consisted of the outer compact hematite layer, the intermediate porous magnetite layer and the inner dense spinel layer. However, on the fireside, the scale consisted of an outer slag-deposit porous layer, an intermediate magnetite layer and an inner spinel layer. Cracks were often observed in the magnetite layer of all specimens and the interface of the matrix/spinel layer, which may cause exfoliation of the oxide scale. The thickness of the hematite and the slag-deposit layer has no significant change with the increase of service time.

Acknowledgement

This work was supported by the National Research Foundation of Korea(NRF) grant funded by the Korea government(MEST) (No. 2011-0030058). The authors acknowledge the provision of specimens by Korea Electric Power Research Institute.

References

1. L. Tan, X. Ren and T. R. Allen, Corro. Sci., **52**, 1520 (2010).
2. K. Natesan and J. H. Park, Int. J. Hydrogen Energy, **32**, 3689 (2007).
3. S. R. J. Saunders, M. Monteiro and F. Rizzo, Prog. Mater. Sci., **53**, 775 (2008).
4. P. Ampornrat and G. S. Was, J. Nucl. Mater., **371**, 1 (2007).
5. S. C. Srivastava and K. M. Godiwalla, J. Mater. Sci., **32**, 835 (1997).
6. K. Song, T. Y. Cho, J. H. Yoon, C. G. Lee, K. Shin, S. H. Lee, K. W. Urm, J. W. Lee and I. S. Kim, Met. Mater. Int., **14**, 721 (2008).
7. Y. Chen, K. Sridharan and T. Allen, Corro. Sci., **48**, 2843 (2006).
8. K. Yin, S. Qiu, R. Tang, Q. Zhang and L. Zhang, J. Supercrit. Fluids, **50**, 235 (2009).
9. L. Tan, Y. Yang and T. R. Allen, Corro. Sci., **48**, 3123 (2006).
10. X. Ren, K. Sridharan and T. R. Allen, J. Nucl. Mater., **358**, 227 (2006).
11. X. Zhong, X. Wu and E. H. Han, J. Supercrit. Fluids, **72**, 68 (2012).
12. Y. He, J. Chang, J. Dong and K. Shin, Adv. Sci. Lett., **4**, 1416 (2011).
13. C. G. Panait, W. Bendick, A. Fuchsmann, A.-F. Gourgues-Lorenzon and J. Besson, Int. J. Pres. Ves. Pip., **87**, 326 (2010).